Sympathetic Ground State Cooling and Time-Dilation Shifts in an $^{27}Al^+$ Optical Clock

J.-S. Chen,[1,2] S. M. Brewer,[1] C. W. Chou,[1] D. J. Wineland,[1,2] D. R. Leibrandt,[1,2,*] and D. B. Hume[1,†]
[1]*Time and Frequency Division, National Institute of Standards and Technology, Boulder, Colorado 80305, USA*
[2]*Department of Physics, University of Colorado, Boulder, Colorado 80309, USA*
(Received 15 August 2016; published 30 January 2017)

We report on Raman sideband cooling of $^{25}Mg^+$ to sympathetically cool the secular modes of motion in a $^{25}Mg^+$-$^{27}Al^+$ two-ion pair to near the three-dimensional (3D) ground state. The evolution of the Fock-state distribution during the cooling process is studied using a rate-equation simulation, and various heating sources that limit the efficiency of 3D sideband cooling in our system are discussed. We characterize the residual energy and heating rates of all of the secular modes of motion and estimate a secular motion time-dilation shift of $-(1.9 \pm 0.1) \times 10^{-18}$ for an $^{27}Al^+$ clock at a typical clock probe duration of 150 ms. This is a 50-fold reduction in the secular motion time-dilation shift uncertainty in comparison with previous $^{27}Al^+$ clocks.

DOI: 10.1103/PhysRevLett.118.053002

Trapped and laser-cooled ions are useful for many applications in quantum information processing and quantum metrology because of their isolation from the ambient environment and the mutual Coulomb interaction [1–6]. The Coulomb interaction establishes normal modes of motion, called secular modes, which enable information exchange and entanglement between ions. For many operations in quantum information processing and metrology, these secular modes should, ideally, be prepared in their ground state. For example, in state-of-the-art trapped-ion optical clocks [7], uncertainty in the Doppler shift due to the residual excitation of these modes is a dominant contribution to the total clock uncertainty [8–10].

All trapped-ion optical clocks to date have been operated with the ions' motion near the Doppler cooling limit [7–10]. For clocks based on quantum-logic spectroscopy of the $^1S_0 \leftrightarrow {}^3P_0$ transition in $^{27}Al^+$ [11], the smallest uncertainty has been achieved by performing continuous sympathetic Doppler cooling on the logic ion ($^{25}Mg^+$) during the clock interrogation [8]. Because of the difficulty of performing accurate temperature measurements of trapped ions near the Doppler cooling limit, the uncertainty of the secular motion temperature was limited to 30% [8].

To reduce the secular motion time-dilation shift and its uncertainty, sub-Doppler cooling techniques can be employed [12–17]. These schemes have not previously been implemented in ion-based clock experiments due to high ambient motional heating rates, the need for extra cooling laser beams, and the difficulty of characterizing the resulting motional state distribution, which can be nonthermal [8,10,18]. For example, in sideband cooling, a nonthermal distribution can result from zero crossings in the cooling transition Rabi rate as a function of the Fock state [19,20] and from cooling durations insufficient to reach equilibrium. Although sideband cooling can reach extremely low energies, a small nonthermal component of the distribution may contribute more than 90% of the total energy [21], rendering the temperature measurement technique using motional sideband ratios unsuitable for determining the energy [12,13].

Here, we demonstrate sympathetic cooling of a $^{25}Mg^+$-$^{27}Al^+$ two-ion pair to the 3D motional ground state with high probability. This is accomplished with Raman sideband cooling, selected for its low cooling limit and experimental convenience. The ion trap used here has motional heating rates less than 12 quanta/s [21], 2 orders of magnitude lower than those achieved in previous $^{27}Al^+$ clocks [8]. The evolution of the Fock-state distribution during the cooling process is investigated by using rate-equation simulations, which is verified by comparison with experimental measurements. The cooling pulse sequence is optimized according to the model. We discuss the various heating mechanisms and the secular motion time-dilation shift uncertainty in this system.

One $^{25}Mg^+$ and one $^{27}Al^+$ are trapped simultaneously in a linear Paul trap to form a pair aligned along the trap (z) axis. The energy levels of $^{25}Mg^+$ and laser beam geometry are shown in Fig. 1. Mutually orthogonal directions x and y are transverse to z. Along each axis there are two motional modes, the "common" (COM) mode where mode vectors of the two ions are in the same direction and the "stretch" (STR) mode where they are opposed. Our trap is operated with axial mode frequencies of 2.7 MHz (COM) and 4.8 MHz (STR) and transverse mode frequencies in the range of 5 to 7.5 MHz [21]. We begin each experiment with 2 ms of Doppler cooling on the $^{25}Mg^+ |\downarrow\rangle \equiv |^2S_{1/2}, F = 3, m_F = -3\rangle \leftrightarrow |^2P_{3/2}, F = 4, m_F = -4\rangle$ cycling transition to cool all motional modes close to the Doppler limit and prepare $^{25}Mg^+$ in $|\downarrow\rangle$. The subsequent sideband cooling and motional state diagnosis are implemented with stimulated Raman transitions between the $|\downarrow\rangle$ and $|\uparrow\rangle \equiv |^2S_{1/2}, F = 2, m_F = -2\rangle$ states. For efficient cooling of all modes, we employ two sets of Raman beams [Fig. 1(a)].

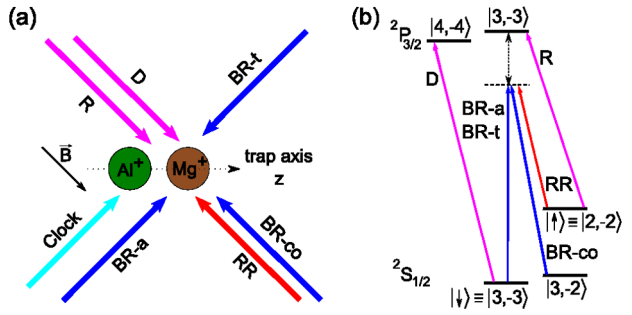

FIG. 1. (a) Geometry of laser beams. (b) $^{25}Mg^+$ energy level diagram (not to scale). Quantum states $|F, m_F\rangle$ are labeled by the total angular momentum F and the projection along the quantization direction m_F. The Raman laser detuning from the transition $|\downarrow(\uparrow)\rangle \leftrightarrow |^2P_{3/2}, F = 3, m_F = -3\rangle$ is approximately 50 GHz, and the magnetic field is about 1 G. D, Doppler cooling; R, repumping; RR, red Raman; BR-a, axial blue Raman; BR-t, transverse blue Raman; BR-co, copropagating blue Raman. (Clock) $^{27}Al^+$ laser beam driving the $^1S_0 \leftrightarrow {}^3P_0$ clock transition.

The axial (BR-a) and transverse (BR-t) blue Raman beams in combination with the red Raman beam (RR) generate the differential wave vectors to cool the axial and transverse modes of motion, respectively. Raman laser beams are transmitted through optical fibers for mode filtering and reduction of beam-pointing fluctuations [27]. Raman "carrier" pulses denote transitions with no change in motional quanta, while red-sideband (RSB) and blue-sideband (BSB) pulses correspond to $|\downarrow, n\rangle \rightarrow |\uparrow, n - \Delta n\rangle$ and $|\downarrow, n\rangle \rightarrow |\uparrow, n + \Delta n\rangle$ transitions, respectively, where n is the initial Fock state and Δn, the order of the sideband transition, represents the number of quanta changed in a single pulse. After a RSB cooling transition, $^{25}Mg^+$ is in $|\uparrow\rangle$, which is then optically pumped to $|\downarrow\rangle$ by applying a pulse sequence with three pulses that drive the $|\uparrow\rangle$ to a $|^2P_{3/2}, F = 3, m_F = -3\rangle$ transition, between which are inserted two Raman carrier pulses that drive the $|^2S_{1/2}, F = 3, m_F = -2\rangle$ to an $|\uparrow\rangle$ transition by applying RR and BR-co simultaneously. The $^{25}Mg^+$ atomic state is determined at the end of each experiment by collecting photons scattered from the cycling transition and converting the photon count histogram to the transition probability [21].

In general, when the Lamb-Dicke limit is not rigorously satisfied, resolved sideband cooling becomes complicated due to the presence of Fock-state population "traps" where the Rabi rate of the RSB transition approaches zero [19,20]. For example, the first order RSB Rabi rate for the z-COM mode (Lamb-Dicke parameter, $\eta = 0.18$) nearly vanishes for $n = 44$. Numerical simulations indicate that the second order RSB pulses are significantly more efficient at reducing populations in high Fock states, depending on the Lamb-Dicke parameter and the time for repumping during each cooling cycle. Multiple second order RSB cooling pulses are applied before the first order RSB pulses for the two axial modes in our experiment [21]. After sideband cooling, all RSB signals nearly vanish, indicating the two-ion pair is close to the 3D motional ground state [21].

Residual motional excitation can be determined by measuring the ratio of the BSB and RSB transition probabilities [12,13]. However, this method is accurate only in thermal equilibrium, which is generally not true after sideband cooling [28]. To overcome this problem, we develop a rate-equation model to simulate the sideband cooling process. We model the cooling dynamics using the coherent RSB transition probability [29]

$$P_{\uparrow,n}(t) = \frac{1}{2}[1 - e^{-\gamma t}\cos(2\Omega_{n,n+\Delta n}t)]P_{\downarrow,n+\Delta n}(0), \quad (1)$$

where Δn is the order of the RSB pulse, $\Omega_{n,n+\Delta n}$ is the Rabi rate for the transition $|\downarrow, n + \Delta n\rangle \rightarrow |\uparrow, n\rangle$, γ is the decoherence rate, and t is the pulse duration. Following Ref. [30], we treat the heating as an interaction with a thermal reservoir. We validate our model by comparing it with experimental data at intermediate times during the cooling sequence. Separate calibrations for the Rabi rates, decoherence rates, and Lamb-Dicke parameters, in combination with the Fock-state distributions from our simulation, are used to produce Rabi-oscillation curves of the secular motion along the z direction for a single $^{25}Mg^+$ with no free parameters. As shown in Fig. 2, Rabi oscillations from our simulation yield good agreement with experimental data throughout the sideband cooling process. Simulations also reveal the nonthermal distribution after sideband cooling [21], and they indicate that the energy of ions after sideband cooling may be underestimated by orders of magnitude in certain situations if it is determined using the BSB-RSB ratio method.

During the sideband cooling process, ions experience recoil from both Raman and repumping pulses. The recoil heating due to Raman beams arises from transitions through the $|^2P_{3/2}\rangle$ excited states [31]. The heating rate due to Raman scattering is estimated to be $<10^{-4}$ quanta/μs for each motional mode [21], both theoretically and via calibration experiments on a single $^{25}Mg^+$ for a given Raman beam intensity [32]. The Rayleigh scattering rate due to the Raman beams is estimated to be 50% of the Raman scattering rate [31]. The resulting heating is independent of the frequency difference between Raman beams, and all motional modes will heat each time the Raman beams are applied to the ions. For this reason, while the heating rates are small, this mechanism contributes significantly to the ions' final energy.

The recoil heating in the repumping sequence is measured by preparing ions in the motional ground state and then applying a carrier pulse followed by a repumping sequence multiple times. This heating scales with η^2 and is about 0.027 quanta per cycle in the z-COM mode. Although this value is relatively large, the effective heating

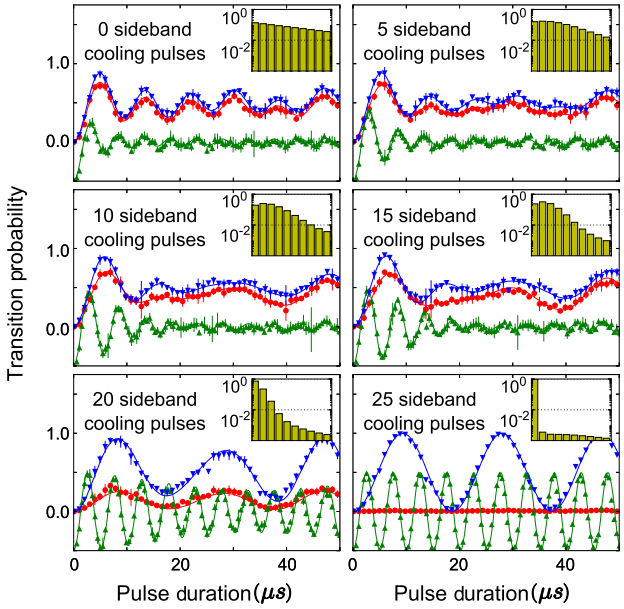

FIG. 2. Rabi oscillations of the first RSB (red, circle), the first BSB (blue, down triangle), and carrier (green, up triangle). Raman transitions of the axial mode for a single $^{25}Mg^{+}$ after different numbers of pulses in the sideband cooling sequence. Carrier Rabi-oscillation curves are shifted by −0.5 for visibility. The cooling sequence consists of 17 second order RSB pulses followed by eight first order RSB pulses to prepare the ion near the motional ground state. Solid lines are given by the rate-equation simulation without any free parameters [21]. The simulated population evolution of the first ten Fock states during the cooling process are shown in the insets. We include 150 Fock states in the simulation.

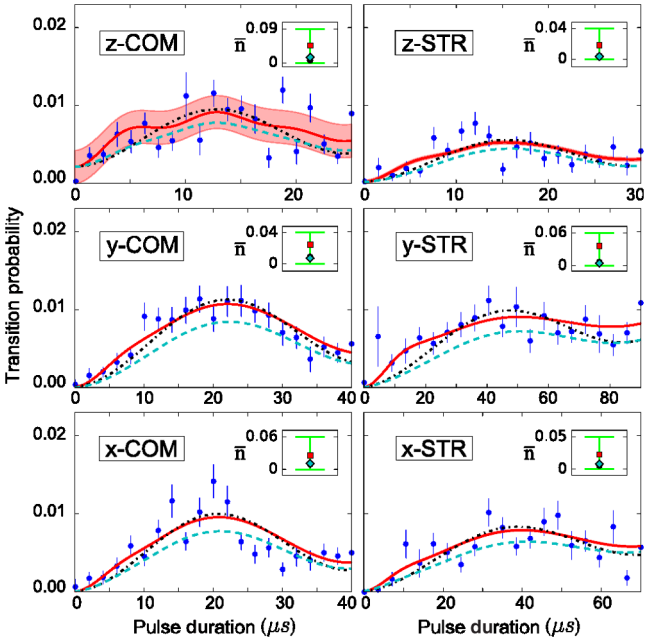

FIG. 3. Red-sideband Rabi oscillations on the $|\downarrow\rangle \rightarrow |\uparrow\rangle$ transition of $^{25}Mg^{+}$ for the six $^{25}Mg^{+}$-$^{27}Al^{+}$ motional modes after Raman sideband cooling. The blue data points are the average of about 50 000 experiments, and the error bars are the standard deviation of the mean. Solid line, double-thermal distribution fit; dotted line, single-thermal distribution fit; dashed line, rate-equation simulation. The red shaded regions represent the range of the off-resonant carrier transitions of the double-thermal distribution fit, which is significant for the z-COM mode, but not the other motional modes [21]. The insets represent the average occupation numbers from fits and the simulation. Diamond, rate-equation simulation; circle, single-thermal distribution fit; square, double-thermal distribution fit. Circles overlay diamonds to within less than the size of the symbol. The green error bars represent the experimental uncertainties of average occupation numbers after sideband cooling. The upper bound of energy is given by the 95% confidence interval of the double-thermal distribution fit.

due to repumping needs to be multiplied by the probability of the population not in the ground state, which becomes negligible at the end of the sideband cooling process.

Effects of off-resonant coupling to the carrier transition during RSB pulses are discussed in Ref. [13]. For an ion in the motional ground state, the probability of motional excitation due to this mechanism scales as $1/\omega^2$, where ω is the motional frequency. Another important source of heating results from the combination of spontaneous emission due to Raman beams and the RSB pulses. After a spontaneous decay to $|\uparrow\rangle$, the RSB pulse will add one motional quantum to the mode addressed. The probability of motional excitation due to this mechanism depends on the RSB pulse duration and scales as $1/\eta$. This mechanism is only present when Raman transitions are used for sideband cooling; optical transitions are immune to this effect. Heating from electric field noise is measured as $\dot{\bar{n}} \approx 10$ quanta/s and 1 quanta/s for the COM and STR modes, respectively [21]. The heating due to off-resonant coupling to the BSB transitions is not considered in our simulation because of its relatively small transition rate, which scales as η^2/ω^2.

To experimentally constrain the motional energy after Raman sideband cooling, we focus on Rabi oscillations of RSB transitions to investigate the population not in the ground state. Motivated by the simulation results, we fit our experimental data to a linear combination of two thermal distributions [21]. Simulation results, fits, and experimental data are plotted in Fig. 3. The mean occupation number, $\bar{n}$, extracted from different methods and the energy uncertainties after sideband cooling are shown in the insets. The upper bound of this uncertainty is given by the 95% confidence interval of the fit to the double-thermal distribution, which gives the highest energy compared to our simulation and the estimate from the single-thermal distribution fit. The lower bound is set to zero. We do not claim that the double-thermal distribution is a complete description of the experimental data, but we think it provides a conservative upper limit on the time-dilation shift due to the secular motion.

To further verify that all motional modes of the $^{25}Mg^{+}$-$^{27}Al^{+}$ two-ion pair are cooled close to the zero-point

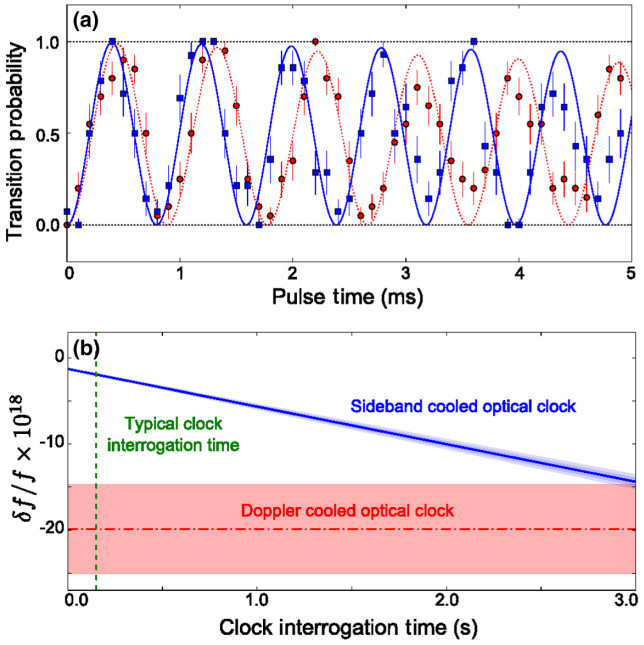

FIG. 4. (a) Rabi oscillation of the $^{27}\mathrm{Al}^{+1}S_0 \leftrightarrow {}^3P_0$ clock transition. Red circles, continuous sympathetic Doppler cooling, $\Omega_{\mathrm{Doppler}} = 2\pi \times 1.126(3)$ kHz; blue squares, 3D sideband cooling, $\Omega_{\mathrm{sc}} = 2\pi \times 1.258(6)$ kHz. Lines are from fitting to an exponential decaying sinusoidal function. (b) Comparison of the secular motion time-dilation shifts in two different clock operating conditions. The solid line and the dash-dotted line represent the fractional frequency shifts, while the shaded regions are uncertainties. For a typical clock interrogation time of 150 ms, the secular motion time-dilation shift of a sideband cooled optical clock is $-(1.9 \pm 0.1) \times 10^{-18}$. The uncertainty of a Doppler cooled optical clock is the sum of the secular motion time-dilation shift, $-(16.3 \pm 5.0) \times 10^{-18}$, and the ac Stark shift from the Doppler cooling light, $-(3.6 \pm 1.5) \times 10^{-18}$ [8].

energy, we compare the Rabi-oscillation frequencies of the $^{27}\mathrm{Al}^{+1}S_0 \leftrightarrow {}^3P_0$ clock transition in two conditions and show the results in Fig. 4(a). We first operate the clock near the Doppler limit by sympathetic Doppler cooling during the clock interrogation [8]. Since the damping rate from the Doppler cooling is much larger than the Rabi rate of the clock transition, the entire Fock-state distribution is averaged over a thermal distribution during a single clock pulse and the Rabi oscillation maintains coherence. In a second experiment, we operate the clock by sideband cooling all motional modes before the clock interrogation pulse. We expect the Rabi rate of the Doppler cooled optical clock ($\Omega_{\mathrm{Doppler}}$) will be 11(2)% smaller than that of the sideband cooled optical clock (Ω_{sc}) due to the Debye-Waller effect [29],

$$\frac{\Omega_{\mathrm{Doppler}}}{\Omega_{\mathrm{sc}}} = \prod_p e^{-\eta_p^2 \bar{n}_p}, \tag{2}$$

where η_p and $\bar{n}_p$ represent the Lamb-Dicke parameter of $^{27}\mathrm{Al}^+$ and the average occupation number at the Doppler limit of the motional mode p, respectively. The uncertainty of the prediction is due to the uncertainty in the motional energy estimation near the Doppler limit. Experimentally, we observe a 10.5(4)% difference between the two clock operating conditions, which agrees with the theoretical prediction.

After preparing ions in the 3D motional ground state, there is no additional cooling light during the clock interrogation, and we can eliminate the associated light shift reported in the previous $^{27}\mathrm{Al}^+$ optical clocks [8]. The average occupation number of the ions in a specific motional mode p during a clock interrogation of duration t_i can be expressed as

$$\langle n_p(t_i) \rangle = \bar{n}_{p,0} + \frac{1}{2}\dot{\bar{n}}_p t_i, \tag{3}$$

where $\bar{n}_{p,0}$ is the energy after sideband cooling given in Fig. 3 and $\dot{\bar{n}}_p$ is the heating rate due to the ambient electric field noise. The angle brackets denote an average over the clock interrogation time. A comparison of the secular motion time-dilation shift using sideband cooling here with continuous Doppler cooling from Ref. [8] is shown in Fig. 4(b). The heating rates of motional modes are the average of measurements spanning several weeks [21]. Using the 2σ uncertainty of our heating rate data to estimate the secular motion time-dilation shift uncertainty, we expect $\delta f/f = -(1.9 \pm 0.1) \times 10^{-18}$ for a 150 ms clock interrogation time [21]. The overall frequency shift is dominated by the zero-point energy, which can be accurately determined, and the uncertainty is dominated by the energy uncertainty after sideband cooling. This is roughly an order of magnitude reduction in the shift and a factor of 50 reduction in the uncertainty due to secular motion time dilation in comparison with $-(16.3 \pm 5.0) \times 10^{-18}$, reported in the previous $^{27}\mathrm{Al}^+$ optical clock [8]. Extending the clock interrogation time to 1 s [33–36], the fractional time-dilation shift due to secular motion is estimated to be $-(5.7 \pm 0.3) \times 10^{-18}$.

In conclusion, we have sympathetically cooled a $^{25}\mathrm{Mg}^+$-$^{27}\mathrm{Al}^+$ two-ion pair to near the 3D motional ground state using stimulated Raman sideband cooling. A rate-equation simulation has been performed to characterize the secular motion energy of the ions in our ion trap, which agrees with experimental data throughout the sideband cooling process. The fractional frequency shift of the $^{27}\mathrm{Al}^+$ $^1S_0 \leftrightarrow {}^3P_0$ clock transition due to secular motion is estimated based on the characterization of ion motion and heating rate measurements. The shift due to secular motion time dilation is reduced by an order of magnitude while the uncertainty is reduced by a factor of 50 in comparison with the previous $^{27}\mathrm{Al}^+$ optical clock. Our model may benefit other experiments utilizing sideband cooling to design efficient cooling pulse sequences.

We thank T. Rosenband for the useful discussions. We thank Y. Lin and T. R. Tan for their careful reading of the manuscript. This work was supported by the Defense Advanced Research Projects Agency and the Office of Naval Research. S. M. B. was supported by the U.S. Army Research Office through MURI Grant No. W911NF-11-1-0400. This Letter is a contribution of the U.S. Government, not subject to U.S. copyright.

*david.leibrandt@nist.gov
†david.hume@nist.gov

[1] R. Blatt and D. J. Wineland, Nature (London) **453**, 1008 (2008).
[2] T. Rosenband, D. B. Hume, P. O. Schmidt, C. W. Chou, A. Brusch, L. Lorini, W. H. Oskay, R. E. Drullinger, T. M. Fortier, J. E. Stalnaker, S. A. Diddams, W. C. Swann, N. R. Newbury, W. M. Itano, D. J. Wineland, and J. C. Bergquist, Science **319**, 1808 (2008).
[3] B. Lanyon, C. Hempel, D. Nigg, M. Müller, R. Gerritsma, F. Zähringer, P. Schindler, J. T. Barreiro, M. Rambach, G. Kirchmair, M. Hennrich, P. Zoller, R. Blatt, and C. F. Roos, Science **334**, 57 (2011).
[4] C. Monroe and J. Kim, Science **339**, 1164 (2013).
[5] T. Esslinger, T. Schaetz, and C. Monroe, New J. Phys. **15**, 085009 (2013).
[6] T. Monz, D. Nigg, E. A. Martines, M. F. Brandl, P. Schindler, R. Rines, S. X. Wang, I. L. Chuang, and R. Blatt, Science **351**, 1068 (2016).
[7] A. D. Ludlow, M. M. Boyd, J. Ye, E. Peik, and P. O. Schmidt, Rev. Mod. Phys. **87**, 637 (2015).
[8] C. W. Chou, D. B. Hume, J. C. J. Koelemeij, D. J. Wineland, and T. Rosenband, Phys. Rev. Lett. **104**, 070802 (2010).
[9] G. P. Barwood, G. Huang, H. A. Klein, L. A. M. Johnson, S. A. King, H. S. Margolis, K. Szymaniec, and P. Gill, Phys. Rev. A **89**, 050501 (2014).
[10] N. Huntemann, C. Sanner, B. Lipphardt, C. Tamm, and E. Peik, Phys. Rev. Lett. **116**, 063001 (2016).
[11] P. O. Schmidt, T. Rosenband, C. Langer, W. M. Itano, J. C. Bergquist, and D. J. Wineland, Science **309**, 749 (2005).
[12] F. Diedrich, J. C. Bergquist, W. M. Itano, and D. J. Wineland, Phys. Rev. Lett. **62**, 403 (1989).
[13] C. Monroe, D. M. Meekhof, B. E. King, S. R. Jefferts, W. M. Itano, D. J. Wineland, and P. Gould, Phys. Rev. Lett. **75**, 4011 (1995).
[14] C. F. Roos, D. Leibfried, A. Mundt, F. Schmidt-Kaler, J. Eschner, and R. Blatt, Phys. Rev. Lett. **85**, 5547 (2000).
[15] G. Manfredi and P.-A. Hervieux, Phys. Rev. Lett. **109**, 255005 (2012).
[16] Y. Lin, J. P. Gaebler, T. R. Tan, R. Bowler, J. D. Jost, D. Leibfried, and D. J. Wineland, Phys. Rev. Lett. **110**, 153002 (2013).
[17] S. Ejtemaee and P. C. Haljan, arXiv:1603.01248.
[18] P. B. R. Nisbet-Jones, S. A. King, J. M. Jones, R. M. Godun, C. F. A. Baynham, K. Bongs, M. Doležal, P. Balling, and P. Gill, Appl. Phys. B **122**, 57 (2016).
[19] G. Poulsen, Y. Miroshnychenko, and M. Drewsen, Phys. Rev. A **86**, 051402(R) (2012).
[20] Y. Wan, F. Gebert, F. Wolf, and P. O. Schmidt, Phys. Rev. A **91**, 043425 (2015).
[21] See Supplemental Material at http://link.aps.org/supplemental/10.1103/PhysRevLett.118.053002, which includes Refs. [22–26], for detailed ions' kinetic energy estimate, and the determination of clock time-dilation shift due to the secular motion.
[22] J. P. Gaebler, T. R. Tan, Y. Lin, Y. Wan, R. Bowler, A. C. Keith, S. Glancy, K. Coakley, E. Knill, D. Leibfried, and D. J. Wineland, Phys. Rev. Lett. **117**, 060505 (2016).
[23] T. J. DiCiccio and B. Efron, Stat. Sci. **11**, 189 (1996).
[24] D. F. V. James, Phys. Rev. Lett. **81**, 317 (1998).
[25] V. V. Dodonov, S. S. Mizrahi, and A. L. de Souza Silva, J. Opt. B **2**, 271 (2000).
[26] D. J. Wineland, W. M. Itano, J. C. Bergquist, and R. G. Hulet, Phys. Rev. A **36**, 2220 (1987).
[27] Y. Colombe, D. H. Slichter, A. C. Wilson, D. Leibfried, and D. J. Wineland, Opt. Express **22**, 19783 (2014).
[28] M. D. Barrett, B. DeMarco, T. Schaetz, V. Meyer, D. Leibfried, J. Britton, J. Chiaverini, W. M. Itano, B. Jelenković, J. D. Jost, C. Langer, T. Rosenband, and D. J. Wineland, Phys. Rev. A **68**, 042302 (2003).
[29] D. J. Wineland, C. Monroe, W. M. Itano, D. Leibfried, B. E. King, and D. M. Meekhof, J. Res. Natl. Inst. Stand. Technol. **103**, 259 (1998).
[30] Q. A. Turchette, C. J. Myatt, B. E. King, C. A. Sackett, D. Kielpinski, W. M. Itano, C. Monroe, and D. J. Wineland, Phys. Rev. A **62**, 053807 (2000).
[31] R. Ozeri, W. M. Itano, R. B. Blakestad, J. Britton, J. Chiaverini, J. D. Jost, C. Langer, D. Leibfried, R. Reichle, S. Seidelin, J. H. Wesenberg, and D. J. Wineland, Phys. Rev. A **75**, 042329 (2007).
[32] W. M. Itano and D. J. Wineland, Phys. Rev. A **25**, 35 (1982).
[33] C. W. Chou, D. B. Hume, M. J. Thorpe, D. J. Wineland, and T. Rosenband, Phys. Rev. Lett. **106**, 160801 (2011).
[34] T. Kessler, C. Hagemann, C. Grebing, T. Legero, U. Sterr, F. Riehle, M. J. Martin, L. Chen, and J. Ye, Nat. Photonics **6**, 687 (2012).
[35] S. Häfner, S. Falke, C. Grebing, S. Vogt, T. Legero, and M. Merimaa, Opt. Lett. **40**, 2112 (2015).
[36] D. B. Hume and D. R. Leibrandt, Phys. Rev. A **93**, 032138 (2016).